Supplementary information for manuscript: Moisture sorption of cellulose-based porous media containing co-solvents and its impact on pore-fiber transport rates of co-solvent solutions

Sajjad Karimnejad and Anton A. Darhuber
Fluids & Flows Group, Department of Applied Physics, Eindhoven University of Technology, Postbus 513, 5600MB Eindhoven, The Netherlands

(Dated: 22 December 2025)

I. MATERIAL PROPERTIES OF CO-SOLVENTS

Table S1 lists the Sigma-Aldrich product number, molecular weight (MW), viscosity (μ_{cs}), and saturated vapor pressure ($p_{cs,vap}$) of the pure co-solvents used in this study.[1–4]

II. VALUES OF THE VAN LAAR COEFFICIENTS

Experimental data of water activity as a function of composition of aqueous co-solvent solutions are available for EGO for a large range of molecular weights.[5–7] However, unfortunately we were unable to find literature data for PEG300. Therefore, we resorted to interpolation of the numerical values of the Van Laar fit parameters A_{12} and A_{21} obtained for MW values above and below 300. The symbols in Fig. S1 represent the available literature data for A_{12}. The solid line is a linear fit, which reproduces the data very well. Interestingly, A_{21} is essentially constant, whereas A_{12} shows a considerable dependence on MW. The interpolated values for PEG300 were found as $A_{12} = -4.43$ and $A_{21} = -0.5$.

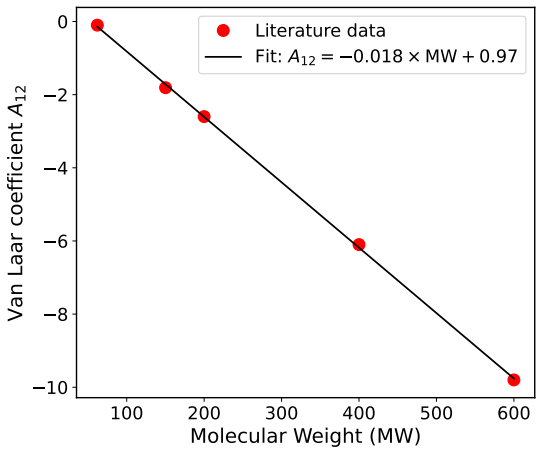

FIG. S1. Numerical values of the Van Laar fit parameter A_{12} for EGOs as a function of molecular weight MW (red circles). The black solid line is a linear fit.

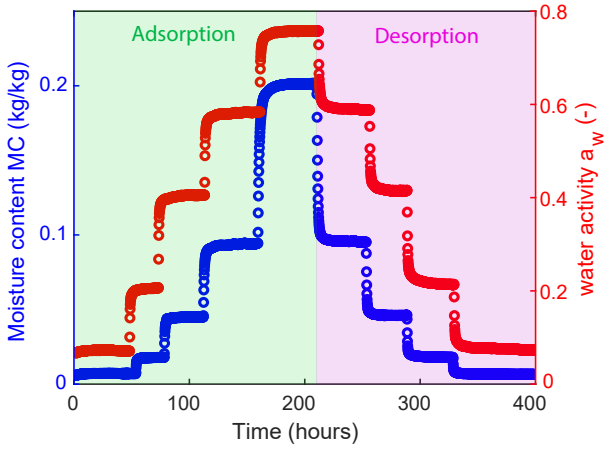

FIG. S2. Water activity a_w (red circles) and moisture content MC of paper C (blue circles) as a function of time. The co-solvent content (PEG300) was $\theta_{cs} = 0.44\,g/g$.

III. TYPICAL EXPERIMENTAL DATA

Figure S2 shows a typical experimental data of the water activity a_w in the measurement chamber and the corresponding moisture content MC of paper C as a function of time.

IV. EQUILIBRIUM MOISTURE SORPTION OF PAPERS B AND C

In Fig. S3, equilibrium moisture sorption isotherms of untreated and co-solvent-infused papers B and C are shown. The filled and open symbols represent the experimental data for adsorption and desorption, respectively. The solid and dashed green lines are corresponding GAB fits for untreated, co-solvent-free papers. The values of the GAB fit parameters for paper B and C are presented in Tab. S2. The solid and dashed red lines represent Eq. (10) in the main manuscript, i.e. the theoretical model according to scenario (1), where we substituted the adsorption/desorption GAB fits of Tab. S2 for $(MC)_{paper}$.

Hysteresis loops between the adsorption and desorption branches are observed for all untreated paper types. Paper C exhibits greater hysteresis than papers A and B. This is consistent with previous observations and was

TABLE S1. Sigma-Aldrich product number, molecular weight MW, viscosity μ_{cs}, and saturated vapor pressure $p_{cs,vap}$ of the pure co-solvents used in this study at 20°C.[1–4]

Co-solvent	Product#	MW	μ_{cs} [mPa s]	$p_{cs,vap}$ [mPa]
Glycerol	449770	92.1	1206	13 ± 5
Ethylene glycol (EG)	324558	62.1	19.8	7728
Tetra(ethylene glycol) (TEG)	110175	194.2	58.3	12 ± 4
PEG300	90878	300	91.0	≤ 0.014

TABLE S2. Adsorption and desorption GAB fit parameter values for untreated papers B and C.

Paper		M_0	C	K
B	Ads.	0.026	6.4	0.90
	Des.	0.032	6.5	0.83
C	Ads.	0.025	3.9	0.86
	Des.	0.039	3.8	0.71

attributed to its high crystallinity and low amorphous content, which limit structural relaxation during moisture cycling.[8] In Fig. S3(b), data of two consecutive adsorption/desorption loops (represented by the green and blue symbols) are shown for untreated paper C, which illustrates that repeated cycling decreases the hysteresis.

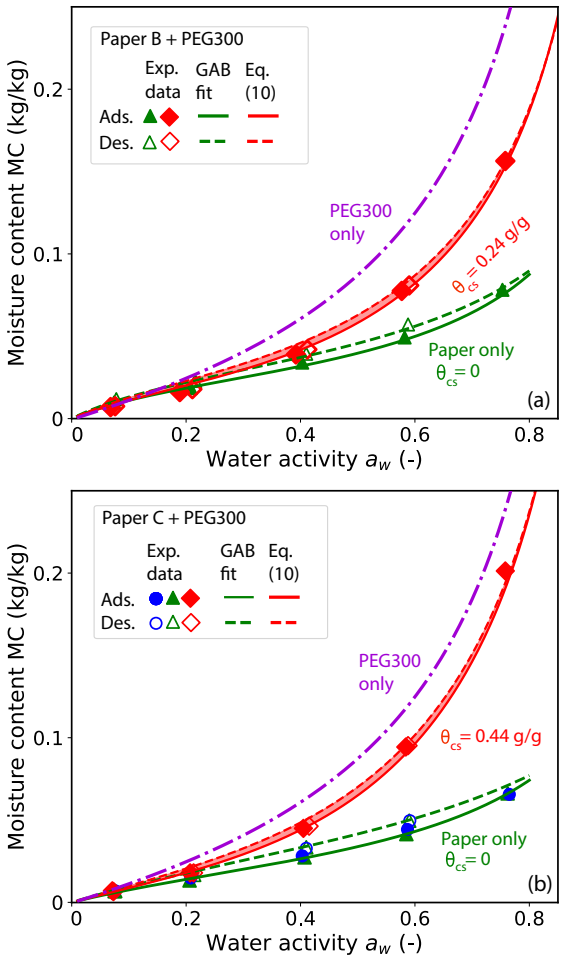

FIG. S3. Equilibrium moisture sorption isotherms for (a) paper B and (b) paper C. The filled and open symbols represent the experimental data for adsorption and desorption, respectively. The green solid and dashed lines are corresponding GAB fits for untreated, co-solvent-free papers. The paper line represents the moisture content of PEG300. The solid and dashed red lines represent Eq. (10) in the main manuscript, i.e. the theoretical model according to scenario (1) for co-solvent-infused papers, where we substituted the adsorption/desorption GAB fits of Tab. S2 for $(MC)_{paper}$.

V. THICKNESS EXPANSION STRAIN

A. Hygroexpansion strain of untreated and co-solvent-infused paper A

Figure S4(a) shows the thickness hygroexpansion strain ϵ_{TD} [defined in Eq. (11) in the main manuscript] of untreated paper A as a function of its moisture content MC. Figure S4(b) illustrates the increment of the thickness hygroexpansion strain [defined by Eq. (12) in the main manuscript] of paper A with an initial PEG300 content of $\theta_{cs,ini} = 0.21$ g/g as a function of water activity a_w.

Chen *et al.* found that there is no hysteresis present in the expansion strain of amorphous cellulose, if it is plotted as a function of the moisture content.[9] In contrast, Fig. S4(a) reveals that considerable hysteresis is observed in the correlation between ϵ_{TD} and MC for paper A. Figure S4(b) illustrates that – similarly to the removal of moisture sorption hysteresis in Fig. 6 – the presence of 0.21 g/g PEG300 suppresses the considerable hygroexpansion strain hysteresis seen with untreated paper A in Fig. 5.

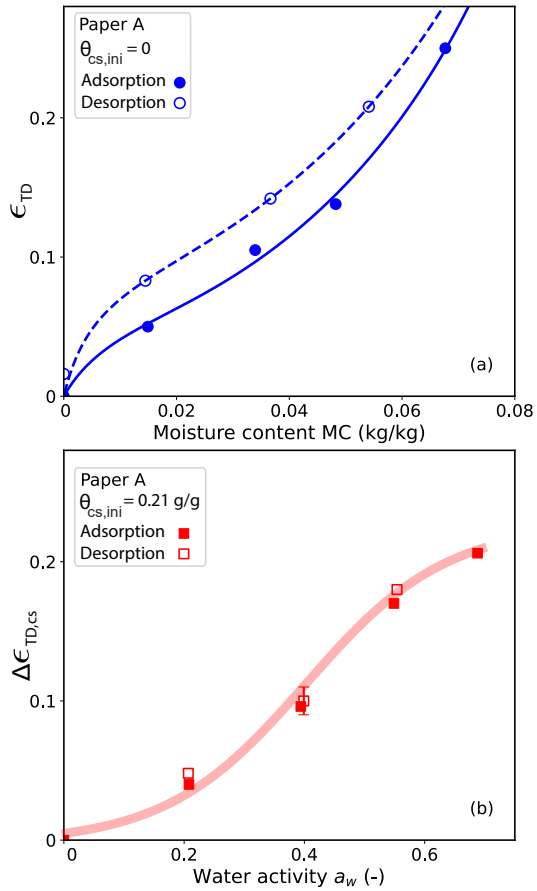

FIG. S4. (a) Thickness hygroexpansion strain ϵ_{TD} of untreated paper A as a function of moisture content MC. (b) Increment of the thickness expansion strain $\Delta\epsilon_{\mathrm{TD,cs}}$ of paper A with initial PEG300 content $\theta_{\mathrm{cs,ini}} = 0.21\,\mathrm{g/g}$ as a function of water activity a_w. Filled and open symbols correspond to experimental data obtained for increasing and decreasing water activities, respectively. All lines are guides to the eye.

B. Increment of thickness expansion strain after model ink deposition

Figure S5 shows the maximum increment of the thickness expansion strain $\Delta\epsilon_{\mathrm{TD,max}}$ after deposition of a droplet of a 60 wt% TEG solution on paper A as a function of initial water activity a_w. Interestingly, $\Delta\epsilon_{\mathrm{TD,max}}$ is essentially independent of a_w, except for the data-point at zero ambient humidity.

VI. THE BERENS & HOPFENBERG MODEL

The Berens & Hopfenberg model[10] considers solvent uptake by polymer layers. It accounts for both solvent diffusion and structural relaxations of the polymers chains, e.g. as a consequence of solvent-induced plasticization.[10,11] In the case of paper and water or co-solvents, liquid uptake is accompanied by substantial

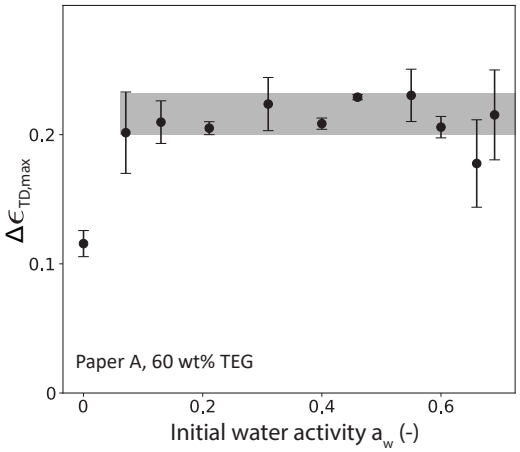

FIG. S5. Maximum increment of the thickness expansion strain $\Delta\epsilon_{\mathrm{TD,max}}$ after deposition of a droplet of a 60 wt% TEG solution on paper A as a function of initial water activity a_w.

swelling. Thus, monitoring changes of the paper thickness provides information about the dynamics of pore-fiber transport.

The increment of the time-dependent expansion strain $\Delta\epsilon_{\mathrm{TD}}(t)$ is modeled as the superposition of a Fickian diffusion term and a relaxation component

$$\Delta\epsilon_{\mathrm{TD}}(t) = \Delta\epsilon_{\mathrm{diff}}(t) + \Delta\epsilon_{\mathrm{relax}}(t). \tag{1}$$

Diffusion Term

The strain contribution as a consequence of solvent diffusion is given by the classical (truncated) Fourier series solution[11]

$$\Delta\epsilon_{\mathrm{diff}}(t) = A_d\left[1 - \frac{8}{\pi^2}\sum_{n=0}^{N}\frac{\exp\left(-(2n+1)^2 k_d t\right)}{(2n+1)^2}\right], \tag{2}$$

where A_d is the strain amplitude and $k_d \equiv 1/t_d$ the diffusion rate constant. We truncated the Fourier series at $N = 20$, which provides a sufficiently accurate approximation.

Relaxation Term

The strain contribution due to relaxation of the cellulose polymer chains is modeled by a sum of exponential functions

$$\Delta\epsilon_{\mathrm{relax}}(t) = \sum_{i=1}^{m} A_{ri}\left(1 - e^{-t/t_{ri}}\right), \tag{3}$$

where A_{ri} and t_{ri} are the amplitude and characteristic time of the i-th relaxation mode. We restrict ourselves to the cases $m = 1$ (for the EG data in Figs. 8 and 9 and

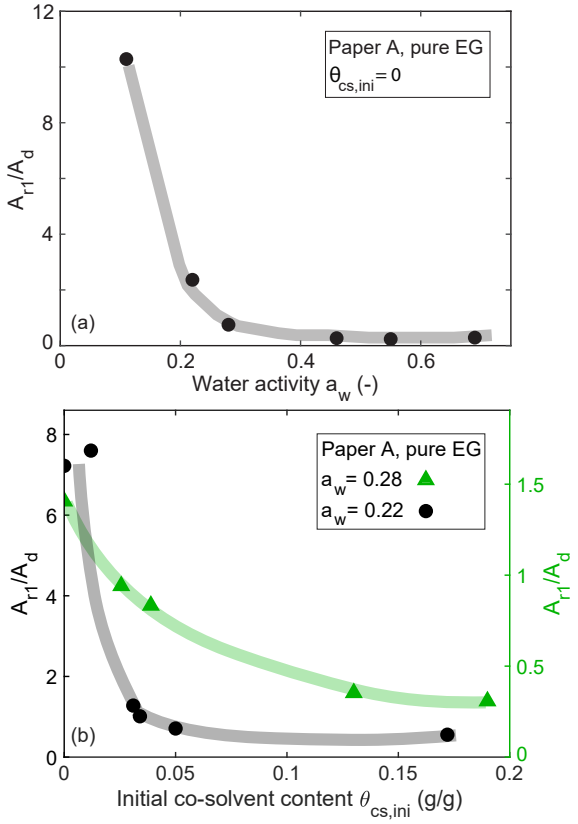

FIG. S6. Ratio of the strain amplitude factors A_{r1}/A_d after deposition of a droplet ($V = 1\,\mu$l) of pure EG on paper A as a function of (a) water activity a_w for $\theta_{\mathrm{cs,ini}} = 0$ and (b) initial EG content $\theta_{\mathrm{cs,ini}}$ for two values of the ambient water activity $a_w = 0.22$ (circles) and 0.28 (triangles). All lines are guides to the eye.

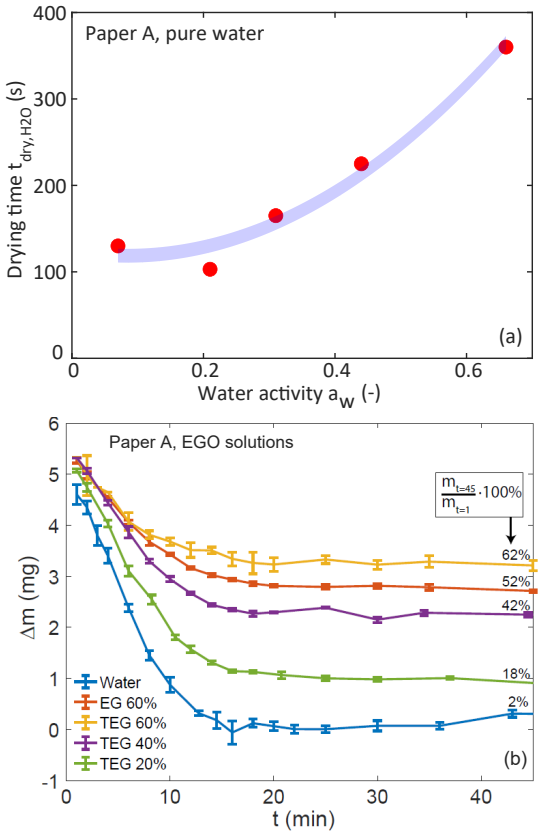

FIG. S7. (a) Drying time $t_{\mathrm{dry,H2O}}$ of a droplet ($V = 1\,\mu$l) of pure water deposited on paper A as a function of water activity a_w. The solid line is a guide to the eye. (b) Mass increment of a sheet of paper A after deposition of droplets of aqueous EGO solutions ($V = 5\,\mu$l) of different concentrations as a function of time ($T = 24°$C and $a_w = 0.3 \pm 0.05$). Plot reproduced from Ref. [17].

the 60 wt% TEG data in Fig. 7 for $a_w < 0.5$) and $m = 2$ (for the 60 wt% TEG data in Fig. 7 for $a_w > 0.5$).

For all cases considered in this study, we found that $t_d < t_{r1} < t_{r2}$, i.e. the diffusion timescale is (typically much) shorter than the relaxation timescales.

VII. RATIO OF STRAIN AMPLITUDE FACTORS

The parameter A_d quantifies the contribution to the total strain resulting from diffusion-driven swelling, associated with the initial ingress of co-solvent and water into the paper fibers due to concentration gradients. The amplitude A_r represents the strain arising from viscoelastic relaxation, which occurs after the initial ingress of liquid that plasticizes the polymer matrix. Figure S6(a,b) presents the ratio of the strain amplitude factors A_{r1}/A_d after deposition of a droplet ($V = 1\,\mu$l) of pure EG on paper A as a function of water activity a_w and initial EG content $\theta_{\mathrm{cs,ini}}$.

Figure S6 shows that the ratio of strain amplitudes A_{r1}/A_d decreases sharply with increasing water activity a_w and with initially present co-solvent content $\theta_{\mathrm{cs,ini}}$. At low values of a_w or $\theta_{\mathrm{cs,ini}}$, the ratio A_{r1}/A_d exceeds 1, suggesting that the response to swelling is primarily driven by internal structural relaxation of the paper matrix. In contrast, as a_w or $\theta_{\mathrm{cs,ini}}$ increase, the paper matrix is substantially pre-swollen (see Fig. 5) and more compliant,[12–16] and the strain response as a consequence of ink deposition is increasingly governed by diffusion, as reflected by the ratio A_{r1}/A_d falling below 1.

VIII. WATER DRYING TIME AS A FUNCTION OF WATER ACTIVITY

Figure S7(a) shows the drying time $t_{\mathrm{dry,H2O}}$ after deposition of a droplet ($V = 1\,\mu$l) of pure water on paper A as a function of water activity a_w. The drying time is defined as the time at which the strain increment $\Delta\epsilon_{\mathrm{TD}}$ decreased to 37% of its maximum value $\Delta\epsilon_{\mathrm{TD,max}}$.

Figure S7(b) shows the mass increment $\Delta m(t)$ of a sheet of paper A after deposition of droplets of aqueous EGO solutions ($V = 5\,\mu$l) of different concentrations as a function of time. The drying time t_{dry} required for water

to evaporate is approximately independent of the EGO type and concentration.

IX. MULTI-COMPONENT SOLUTIONS

A. Pore-fiber transport of quaternary solutions

Figure S8 shows the overall characteristic swelling timescale $t_{0.63}$ of paper A after deposition of a 1 μl droplet of a 60 wt% TEG solution containing 3.6 wt% $MgCl_2$ as a function of the initial SDS concentration c_{SDS}. Measurements were taken at two different water activities $a_w = 0.42$ and 0.67. For both values of a_w, $t_{0.63}$ decreases with increasing SDS concentration and remains constant for $c_{SDS} \gtrsim 2.5$ wt%. The effect of relative humidity on the pore-fiber transport rate is consistent with the behavior of the ternary solutions discussed in the main manuscript.

B. Concentration-dependence of the viscosity and surface tension of TEG solutions

Viscosity measurements were performed using a concentric-cylinder viscometer (Brookfield II+Pro), while surface tensions of the solutions were determined with a Wilhelmy plate (NIMA, PTP-10) in combination with a precision scale (Kern, ALT 220-5DAM). Experiments were conducted at a water activity of $a_w = 0.33 \pm 0.03$ and a temperature of 22 ± 1°C.

Figure S9 shows the viscosity μ of 60 wt% TEG with $MgCl_2$ as a function of the $MgCl_2$ concentration c_{MgCl_2}. In this concentration range, we found that the surface tension γ remains essentially constant at 51 ± 0.2 mN/m. Table S3 shows γ and μ of 60 wt% TEG containing 3.6 wt% $MgCl_2$ and SDS as a function of the SDS concentration c_{SDS}.

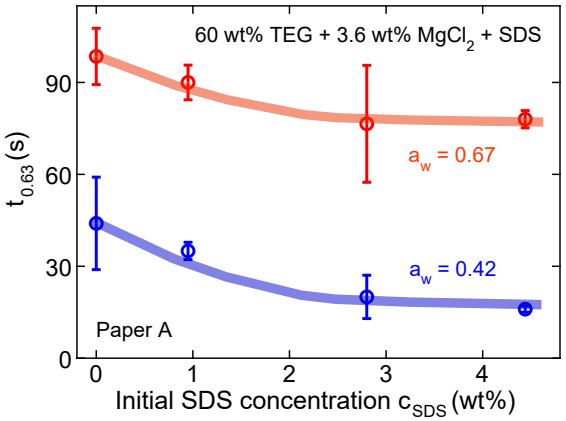

FIG. S8. Overall characteristic swelling timescale $t_{0.63}$ of paper A after deposition of a 1 μl droplet of a 60 wt% TEG solution containing 3.6 wt% $MgCl_2$ as a function of the initial SDS concentration c_{SDS}. Solid lines are guides to the eye.

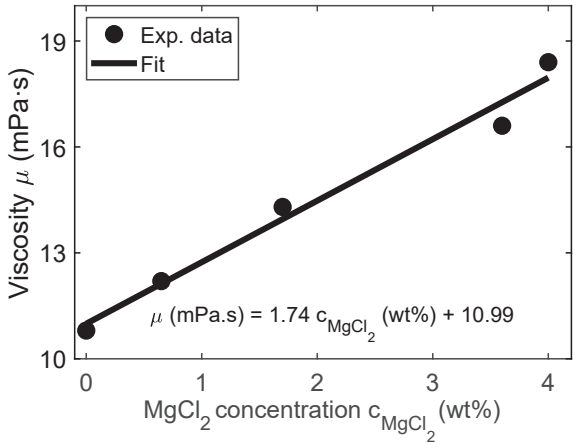

FIG. S9. Viscosity μ of a ternary system consisting of an aqueous 60 wt% TEG solution and $MgCl_2$ as a function of the $MgCl_2$ concentration c_{MgCl_2}.

TABLE S3. Surface tension γ and viscosity μ of a quaternary system consisting of an aqueous 60 wt% TEG solution, 3.6 wt% $MgCl_2$ and SDS as a function of the SDS concentration c_{SDS}.

c_{SDS} (wt%)	0	0.95	4.44
γ (mN/m)	51	37.47	36.64
μ (mPa·s)	16.5	16.8	19.7

REFERENCES

[1] U. K. Krieger, F. Siegrist, C. Marcolli, E. U. Emanuelsson, F. M. Gøbel, M. Bilde, A. Marsh, J. P. Reid, A. J. Huisman, I. Riipinen, N. Hyttinen, N. Myllys, T. Kurtén, T. Bannan, C. J. Percival and D. Topping, *Atmos. Meas. Tech.*, 2018, **11**, 49–63.

[2] S. P. Verevkin, D. H. Zaitsau, V. N. Emel'yanenko and A. A. Zhabina, *Fluid Phase Equilibria*, 2015, **397**, 87–94.

[3] The Dow Chemical Company, *Tetraethylene Glycol Product Information*, `https://www.dow.com`, 2003, Technical data sheet.

[4] MEGlobal, *Monoethylene Glycol Product Guide*, `https://www.meglobal.biz`, 2008, Technical brochure.

[5] L. Ninni, M. S. Camargo and A. J. A. Meirelles, *Thermochim. Acta*, 1999, **328**, 169–176.

[6] M. Herskowitz and M. Gottlieb, *J. Chem. Eng. Data*, 1984, **29**, 173–175.

[7] *MonoEthylene Glycol product guide*, MEGlobal, 2008.

[8] C. A. S. Hill, A. Norton and G. Newman, *J. Appl. Polym. Sci.*, 2009, **112**, 1524–1537.

[9] M. Chen, B. Coasne, R. Guyer, D. Derome and J. Carmeliet, *Nat. commun.*, 2018, **9**, 3507.

[10] A. Berens and H. Hopfenberg, *Polymer*, 1978, **19**, 489–496.

[11] J. Crank, *The Mathematics of Diffusion*, Oxford University Press, 1975.

[12] K. C. Yeh, J. M. Considine and J. C. Suhling, *Proc. Tappi Int. Pap. Phys. Conf. (Kona, Hawaii)*, 1991, 695–711.

[13] M. Lee, S. Kim, H.-Y. Kim and L. Mahadevan, *Phys. Fluids*, 2016, **28**, 042101.

[14] J.-W. Rhim, *Food Sci. Biotechnol.*, 2010, **19**, 243–247.
[15] B. Lin, J. Auernhammer, J.-L. Schäfer, T. Meckel, R. Stark, M. Biesalski and B.-X. Xu, *Cellulose*, 2022, **29**, 1129–1148.
[16] W. J. Cousins, *Wood Sci. Technol.*, 1978, **12**, 161–167.
[17] M. G. Wijburg, *Transport and Evaporation of Aqueous Co-solvent Solutions in Thin Porous Media*, MSc thesis, Eindhoven University of Technology, 2022.